Supporting Information

Highly stable and efficient photoelectrochemical water oxidation at an anisotropically crystallized monoclinic WO_3 film with predominant growth of (202) plane

Hau H. Ho,[a] Zaki N. Zahran,[a] Debraj Chandra,[a] Tomohiro Katsuki,[a] Yuta Tsubonouchi,[a] Norihisa Hoshino,[a] Hidenobu Shiroishi,[b] Manabu Ishizaki,[c] Masato Kurihara,[c] Hung M. Chu,[d] Hoa D. Nguyen,[d] and Masayuki Yagi [a*]

[a] Department of Materials Science and Technology, Faculty of Engineering, Niigata University, 8050 Ikarashi-2, Niigata 950-2181, Japan.

[b] National Institute of Technology, Tokyo College, Kunugida 1220-2, Hachioji, Tokyo 193-0997, Japan

[c] Faculty of Science, Yamagata University, 1-4-12 Kojirakawa-machi, Yamagata 990-8560, Japan.

[d] School of Materials Science and Engineering, Hanoi University of Science and Technology (HUST), No 1, Dai Co Viet Street, Hanoi, Vietnam.

[*]Corresponding author: yagi@eng.niigata-u.ac.jp

Contents:

Figure S5. XRD patterns of the WO_3(*w*-Oxa) electrode before and after bulk photoelectrolysis.

Table S1. Comparison of performances of state-of-the-art WO_3 photoanodes for PEC water oxidation.[a)]

Structures	Electrolyte	pH	$IPCE_{420}$ (%)	η_{sep} (%)	η_{cat} (%)	FE_{O2} (%)	Stability: Initial current (mA cm^{-2})	Stability: Current decrease	Ref.
WO_3(*w*-Oxa)	1.0 M $HClO_4$	0	38	50 [k)]	95 [k)]	95 [l)]	0.98	Remained constant for 7 h and then, decreased by 5 % for 20 h. [l)]	This work
WO_3 with a (021) facet	0.1 M $NaClO_4$	na	na	na	na	95	0.65	Remained constant for 36 h.	S1
WO_3 nanoplate with (200) and (002) facets	0.1 M H_2SO_4	0.7	47	na	na	na	3.71	Decreased by 23 % for 0.28 h.	S2
Hierarchical 3D self-supporting WO_3 micro-nano	0.1 M H_2SO_4	0.7	na	na	na	82	1.2	Remained constant for 2 h.	S3
WO_3 nanoflakes	1.0 M H_2SO_4	0	10	na	na	na	na	na	S4
WO_3 hexagonal prism	1.0 M $HClO_4$	0	47	na	na	70 [l)]	1.0	Decreased by 25 % for 5 h. [l)]	S5
Sandwich structured WO_3 nanoplatelets	0.1 M Na_2SO_4	7.1	70	64	90	85	3.0	Decreased by 10 % for 5 h.	S6
WO_3 nanoparticles	0.1 M Na_2SO_4	7	na	na	na	na	2.0	Decreased by 85 % for 0.5 h.	S7
WO_3 nanorod	0.5 M Na_2SO_4	na	15	na	na	na	na	na	S8
WO_3 nanosheets	0.5 M Na_2SO_4	na	na	na	na	na	1.7	Remained constant for 1 h and then, decreased by 16 % for 3 h.	S9
Terrace-like WO_3	0.5 M Na_2SO_4	7.2	10	23	na	na	3.0	Decreased by 60 % for 11 h.	S10
WO_{3-x} with oxygen vacancy	0.1 M Tris-PBS	7.0	na	32	na	na	0.45	Decreased by 55 % for 24 h.	S11
N_2-intercalated WO_3 Nanorod	0.1 M phosphate buffer	6	43.6 [b)]	na	na	na	0.8	Decreased by 25 % for 0.08 h.	S12
Mesoporous WO_3	0.1 M phosphate buffer	6	36 [b)]	na	na	75	0.8	Decreased by 50 % for 1 h.	S13
WO_3 nanoflake	0.25 M phosphate buffer	na	15	na	na	na	1.8	Decreased by 30 % for 0.08 h.	S14

Nanoporous WO_3	0.5 M Na_2SO_4	7	na	53	50	na	na	na	S15
WO_3 with oxygen vacancy	0.1 M PBS	7	18	na	na	88	2.7	Decreased by 8 % for 0.11 h.	S16
WO_3 nanoplate	0.1 M Na_2SO_4	7.1	38	na	na	na	1.7	Remained constant for 1.11 h.	S17
Pore-Rich WO_3 Ultrathin Nanosheets	0.5 M Na_2SO_4	6.6	na	na	na	na	2.14	Remained constant for 0.8 h.	S18
N_2-intercalated mesoporous WO_3	0.1 M phosphate buffer	6.0	25.4 [b)]	na	na	66 [l)]	0.42	Remained constant for 0.16 h and then, decreased by 25 % for 1 h. [l)]	S19
WO_3 nanorods	0.5 M Na_2SO_4	na	18 [c)]	na	na	na	na	na	S8
WO_3 nanowires	0.1 M Na_2SO_4	na	4	na	na	na	na	na	S20
WO_3 nanoflakes	0.1 M Na_2SO_4	na	22	na	na	na	na	na	S20
WO_3 nanorods	0.5 M Na_2SO_4	7	10	na	na	85	0.5	Remained constant for 0.05 h.	S21
WO_3 nanoflakes	0.1 M Na_2SO_4	7	18	na	na	na	na	na	S22
WO_3 nanorods	0.5 M Na_2SO_4	na	7	na	na	na	na	na	S23
WO_3 nanoparticles	1.0 M H_2SO_4	-0.3	25	na	na	na	na	na	S24
WO_3 nanoplates	1.0 M $HClO_4$	0	65 [e)]	na	na	na	na	na	S25
WO_3 mesoporous	1.0 M H_2SO_4	-0.3	38.5 [f)]	na	na	na	na	na	S26
WO_3 nanoporous	0.5 M H_2SO_4	0	18 [g)]	na	na	na	na	na	S27
WO_3 nanowires	0.5 M H_2SO_4	0	35	na	na	na	0.5	Decreased by 15 % for 5 h.	S28
WO_3 nanosheets	0.1 M Na_2SO_4	na	34	na	na	na	na	na	S29
WO_3 spherical nanoparticles	0.5 M H_2SO_4	0.3	5 [h)]	na	na	na	na	na	S30
WO_3 nanoparticles	1 M H_2SO_4	na	5 [i)]	na	na	na	na	na	S31
WO_3 nanoparticles	0.1 M H_2SO_4	0.69	30	na	na	na	0.75	Decreased by 20 % for 1 h.	S22
Colloidal WO_3 nanowires	0.5 M H_2SO_4	na	26	na	na	na	1.9	Decreased by 32 % for 1 h.	S32
WO_3 nanorods with oxygen vacancy	0.5 M Na_2SO_4	6.8	na	63	78	na	2.0	Decreased by 46 % for 1 h.	S33
WO_3 with anodization in citric acid	0.5 M H_2SO_4	na	8 [j)]	na	na	na	0.71	Decreased by 20 % for 1 h.	S34
Thin-layer nanostructured WO_3	1.0 M CH_3SO_3H	na	37	na	na	na	4.0	Remained constant for 20 h.	S35
WO_3 with oxygen vacancy	0.5 M H_2SO_4	na	33	na	na	na	na	na	S36

Tree-like Nanoporous WO_3	0.5 M phosphate buffer	7	25	75	na	55	2.0	Decreased by 30 % for 1 h.	S37
Porous WO_3	0.5 M Na_2SO_4	na	50	na	na	na	na	na	S38
WO_3 plate	0.2 M Na_2SO_4	6.8	8	na	75	80	0.3	Decreased by 40 % for 0.28 h.	S39

[a)] na: not available, measured at 1.23V vs. RHE using simulated solar light (AM 1.5, 100 mW cm^{-2}), [b)] 0.5 V vs. Ag/AgCl (1.05 V vs. RHE), [c)] 0.8 V vs. Ag/AgCl (pH unmentioned), [d)] 1.2 V vs. Ag/AgCl (1.81 V vs. RHE), [e)] 1.0 V vs. RHE, [f)] 1.26 V vs. RHE, [g)] 1.2 V vs. Ag/AgCl (1.4 V vs. RHE), [h)] 1.2 V vs. NHE (pH unmentioned), [i)] 1.5 V vs. SCE (pH unmentioned), [j)] 1.0 V vs. Ag/AgCl (pH unmentioned), [k)] Monoclinic light (LED, 420 nm, 3.75 mW cm^{-2}), [l)] Visible light (Xe lamp with L39 and heat-cut filter, 100 mW cm^{-2}).

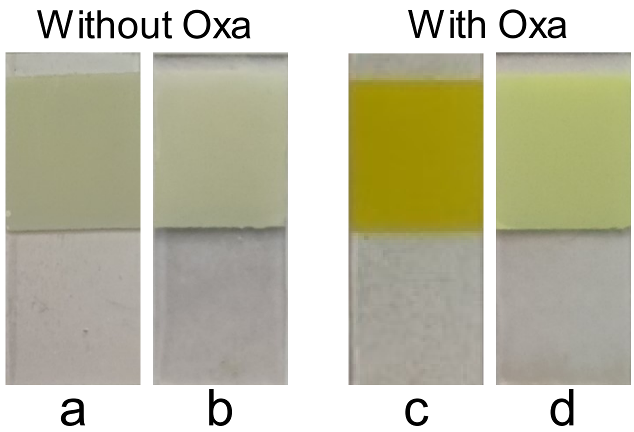

Figure S1. Photos of WO_3 films prepared (a, b) without and (c, d) with Oxa (a, c) before and (b, d) after calcination at 500 ^{o}C.

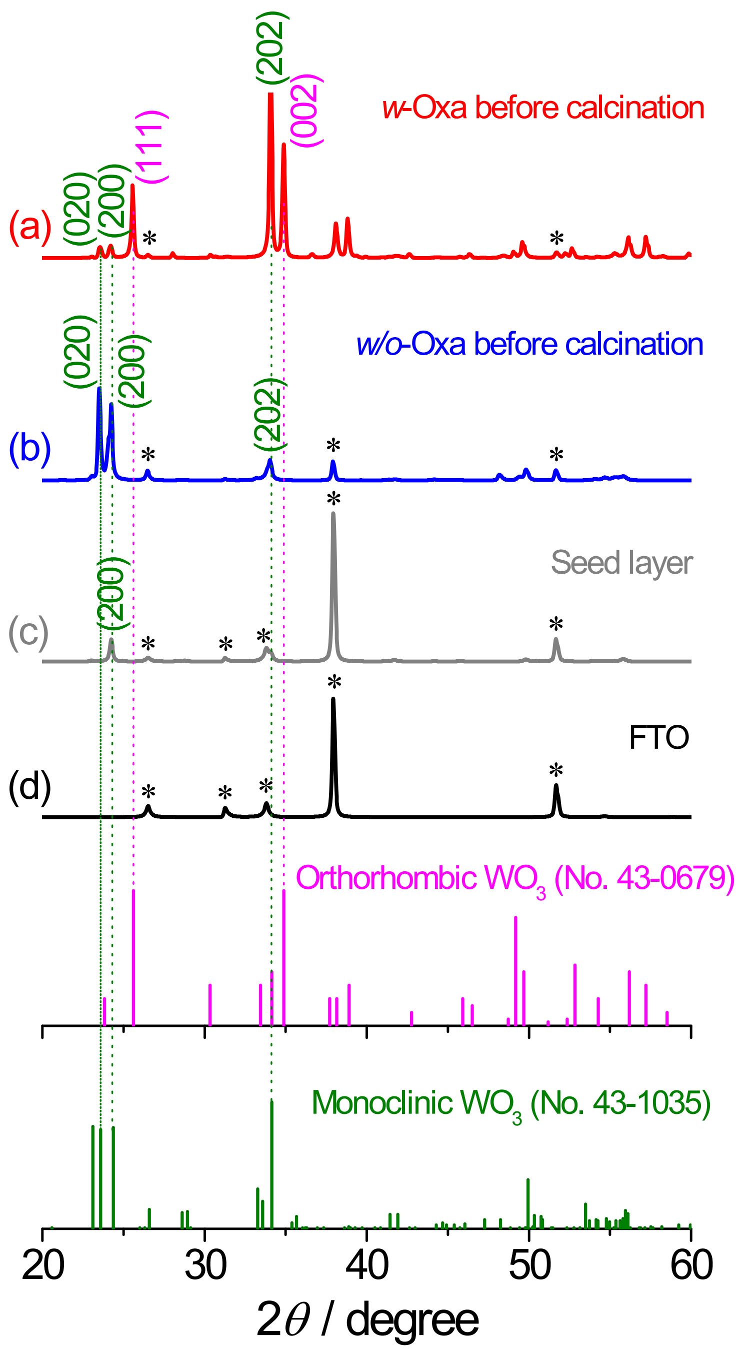

Figure S2. XRD patterns of precursor films deposited (a) with and (b) without Oxa by hydrothermal at 180 ˚C (before calcination), (c) the seed layer on FTO substrates and (d) a bare FTO substrate. The peaks of the FTO substrate are marked by asterisks. PDF data of orthorhombic WO_3 (magenta bars, JCPDF No. 43-0679) and monoclinic WO_3 (green bars, No. 43-1035) are shown in figure, and the planes assigned by orthorhombic and monoclinic WO_3 are indicated by magenta and green, respectively in a and b.

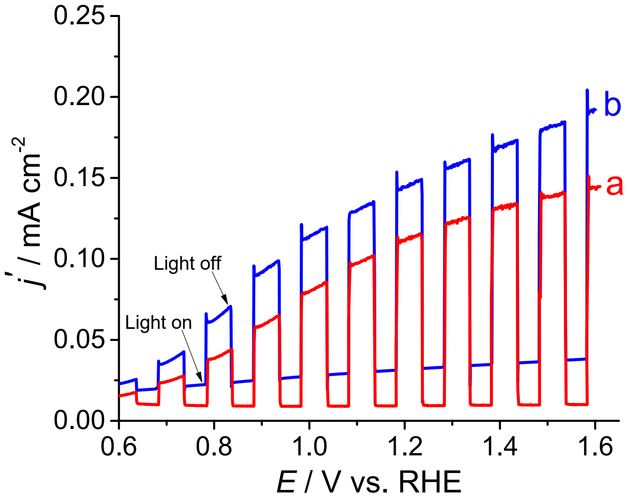

Figure S3. Current density (j') normalized by film thickness-E curves for (a) WO_3(*w*-Oxa) and (b) WO_3(*w/o*-Oxa) electrodes as measured in a 1.0 M $HClO_4$ solution (pH = 0) at a scan rate of 10 mV s^{-1} under chopped visible light illumination (λ > 390 nm, 100 mW cm^{-2}). The j' value was obtained by just dividing the current values by the film thickness.

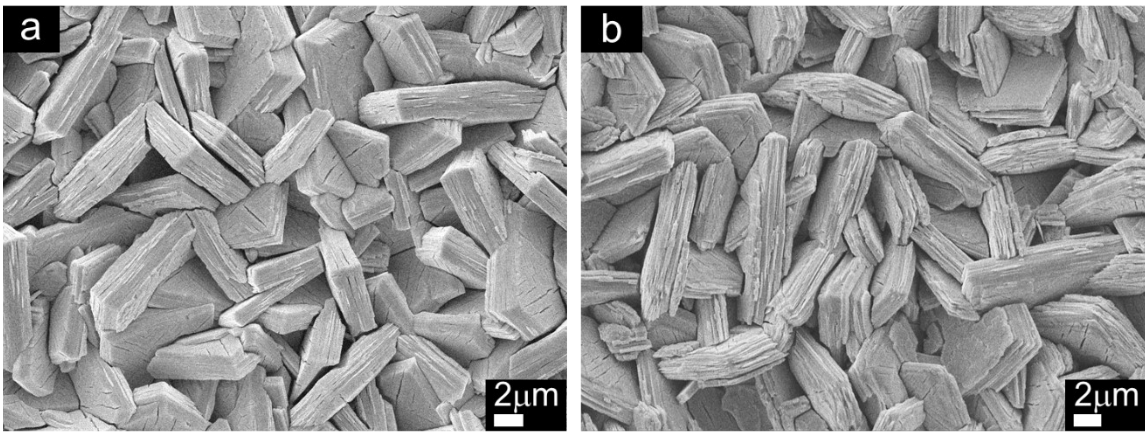

Figure S4. Top-view SEM images of the WO_3(*w*-Oxa) electrode before (a) and after (b) 20 h bulk photoelectrolysis.

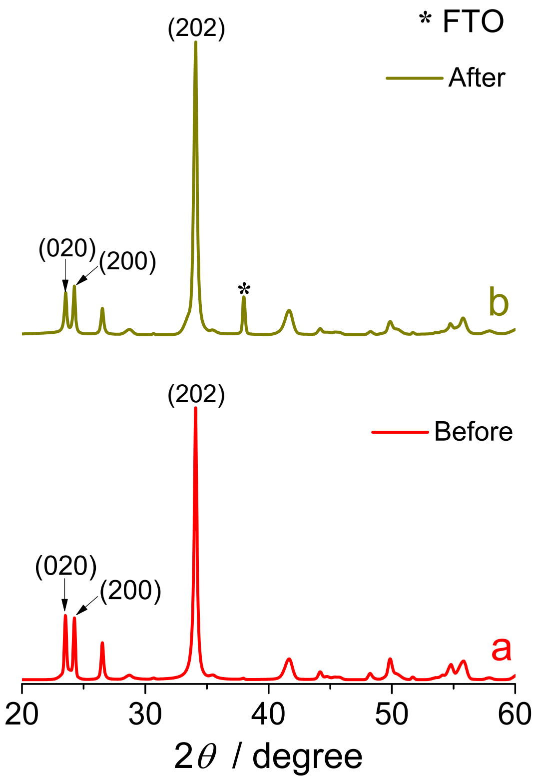

Figure S5. XRD spectra of the WO_3(*w*-Oxa) electrode (a) before and (b) after the 20 h bulk photoelectrolysis. The peaks of the FTO substrate are marked by asterisks.

References

(S1) Shi, X.; Wu, Q.; Cui, C. Modulating WO_3 Crystal Orientation to Suppress Hydroxyl Radicals for Sustainable Solar Water Oxidation. *ACS Catal.* **2023**, *13* (2), 1470–1476. https://doi.org/10.1021/acscatal.2c05325.

(S2) Wang, S.; Chen, H.; Gao, G.; Butburee, T.; Lyu, M.; Thaweesak, S.; Yun, J. H.; Du, A.; Liu, G.; Wang, L. Synergistic Crystal Facet Engineering and Structural Control of WO_3 Films Exhibiting Unprecedented Photoelectrochemical Performance. *Nano Energy* **2016**, *24*, 94–102. https://doi.org/10.1016/j.nanoen.2016.04.010.

(S3) Cai, M.; Fan, P.; Long, J.; Han, J.; Lin, Y.; Zhang, H.; Zhong, M. Large-Scale Tunable 3D Self-Supporting WO_3 Micro-Nano Architectures as Direct Photoanodes for Efficient Photoelectrochemical Water Splitting. *ACS Appl. Mater. Interfaces* **2017**, 9, 21, 17856–17864. https://doi.org/10.1021/acsami.7b02386.

(S4) Li, W.; Da, P.; Zhang, Y.; Wang, Y.; Lin, X.; Gong, X.; Zheng, G. WO_3 Nanoflakes for Enhanced Photoelectrochemical Conversion. *ACS Nano* **2014**, *8* (11), 11770–11777. https://doi.org/10.1021/nn5053684.

(S5) Chandra, D.; Katsuki, T.; Tanahashi, Y.; Togashi, T.; Tsubonouchi, Y.; Hoshino, N.; Zahran, Z. N.; Yagi, M. Temperature-Controlled Transformation of WO_3 Nanowires into Active Facets-Exposed Hexagonal Prisms toward Efficient Visible-Light-Driven Water Oxidation. *ACS Appl. Mater. Interfaces* **2023**, *15* (17), 20885–20896. https://doi.org/10.1021/acsami.2c22483.

(S6) Zheng, G.; Wang, J.; Zu, G.; Che, H.; Lai, C.; Li, H.; Murugadoss, V.; Yan, C.; Fan, J.; Guo, Z. Sandwich Structured WO_3 Nanoplatelets for Highly Efficient Photoelectrochemical Water Splitting. *J. Mater. Chem. A* **2019**, *7* (45), 26077–26088. https://doi.org/10.1039/c9ta09188b.

(S7) Le, H. V.; Pham, P. T.; Le, L. T.; Nguyen, A. D.; Tran, N. Q.; Tran, P. D. Fabrication of Tungsten Oxide Photoanode by Doctor Blade Technique and Investigation on Its Photocatalytic Operation Mechanism. *Int. J. Hydrogen Energy* **2021**, *46* (44), 22852–22863. https://doi.org/10.1016/j.ijhydene.2021.04.113.

(S8) Kalanur, S. S.; Hwang, Y. J.; Chae, S. Y.; Joo, O. S. Facile Growth of Aligned WO_3 Nanorods on FTO Substrate for Enhanced Photoanodic Water Oxidation Activity. *J. Mater. Chem. A* **2013**, *1* (10), 3479–3488. https://doi.org/10.1039/c3ta01175e.

(S9) Mahadik, M. A.; Lee, H. H.; Chae, W. S.; Cho, M.; Jang, J. S. Energy-Efficient Photoelectrochemical Water Splitting and Degradation of Organic Dyes over Microwave-Assisted WO_3 Nanosheets/W Foil with Rapid Charge Transport. *Sol. Energy Mater. Sol. Cells* **2022**, *246* (August), 111939. https://doi.org/10.1016/j.solmat.2022.111939.

(S10) Xia, M.; Zhao, X.; Lin, C.; Pan, W.; Zhang, Y.; Guo, Z.; Leung, D. Y. C. High-Voltage Etching-Induced Terrace-like WO_3 Photoanode for Efficient Photoelectrochemical Water Splitting. *ACS Appl. Energy Mater.* **2023**, *6* (17), 8717–8728. https://doi.org/10.1021/acsaem.3c01164.

(S11) Zhang, C.; Zheng, X.; Ning, Y.; Li, Z.; Wu, Z.; Feng, X. Enhancing Long-Term Stability of Bio-Photoelectrochemical Cell by Defect Engineering of a WO_{3-x} Photoanode. *J. Energy Chem.* **2023**, *80*, 584–593. https://doi.org/10.1016/j.jechem.2023.02.003.

(S12) Chandra, D.; Li, D.; Sato, T.; Tanahashi, Y.; Togashi, T.; Ishizaki, M.; Kurihara, M.; Mohamed, E. A.; Tsubonouchi, Y.; Zahran, Z. N.; Saito, K.; Yui, T.; Yagi, M. Characterization and Mechanism of Efficient Visible-Light-Driven Water Oxidation on an in Situ N_2 - Intercalated WO_3 Nanorod Photoanode. *ACS Sustainable Chem. Eng*. **2019**, 7, 21, 17896–17906 , 1–11. https://doi.org/10.1021/acssuschemeng.9b04467.

(S13) Chandra, D.; Saito, K.; Yui, T.; Yagi, M. Tunable Mesoporous Structure of Crystalline WO_3 Photoanode toward Efficient Visible-Light-Driven Water Oxidation. *ACS Sustainable Chem. Eng*. **2018**, 6, 12, 16838–16846. https://doi.org/10.1021/acssuschemeng.8b04166.

(S14) Rong, Y. Q.; Yang, X. F.; Zhang, W. De; Yu, Y. X. Porous Ultrathin WO_3 Nanoflake Arrays as Highly Efficient Photoanode for Water Splitting. *Mater. Lett.* **2019**, *246*, 161–164. https://doi.org/10.1016/j.matlet.2019.03.044.
(S15) Wang, A.; Cao, D.; Zhang, F.; Chen, Y.; Feng, J.; Fang, D.; Mi, B.; Gao, Z.; Li, Z. Ultrathin and Conformal TiOx Overlayers on WO_3 Photoelectrodes for Simultaneous Surface Trap Passivation and Heterojunction Formation. *ACS Catal.* **2024**, 3446–3456. https://doi.org/10.1021/acscatal.3c05876.
(S16) Yan, L.; Dong, G.; Huang, X.; Zhang, Y.; Bi, Y. Unraveling Oxygen Vacancy Changes of WO_3 Photoanodes for Promoting Oxygen Evolution Reaction. *Appl. Catal. B Environ.* **2024**, *345* (January), 123682. https://doi.org/10.1016/j.apcatb.2023.123682.
(S17) Zheng, G.; Jiang, S.; Cai, M.; Zhang, F.; Yu, H. WO_3/FeOOH Heterojunction for Improved Charge Carrier Separation and Efficient Photoelectrochemical Water Splitting. *J. Alloys Compd.* **2024**, *981* (October 2023), 173637. https://doi.org/10.1016/j.jallcom.2024.173637.
(S18) Liu, Y.; Liang, L.; Xiao, C.; Hua, X.; Li, Z.; Pan, B.; Xie, Y. Promoting Photogenerated Holes Utilization in Pore-Rich WO_3 Ultrathin Nanosheets for Efficient Oxygen-Evolving Photoanode. *Adv. Energy Mater.* **2016**, *6* (23), 1–7. https://doi.org/10.1002/aenm.201600437.
(S19) Li, D.; Chandra, D.; Takeuchi, R.; Togashi, T.; Kurihara, M.; Saito, K.; Yui, T.; Yagi, M. Dual-Functional Surfactant-Templated Strategy for Synthesis of an In Situ N_2-Intercalated Mesoporous WO_3 Photoanode for Efficient Visible-Light-Driven Water Oxidation. *Chem. – A Eur. J.* **2017**, *23* (27), 6596–6604. https://doi.org/10.1002/chem.201700088.
(S20) Su, J.; Feng, X.; Sloppy, J. D.; Guo, L.; Grimes, C. A. Vertically Aligned WO_3 Nanowire Arrays Grown Directly on Transparent Conducting Oxide Coated Glass: Synthesis and Photoelectrochemical Properties. *Nano Lett.* **2011**, *11* (1), 203–208. https://doi.org/10.1021/nl1034573.
(S21) Pihosh, Y.; Turkevych, I.; Mawatari, K.; Asai, T.; Hisatomi, T.; Uemura, J.; Tosa, M.; Shimamura, K.; Kubota, J.; Domen, K.; Kitamori, T. Nanostructured WO_3 /$BiVO_4$ Photoanodes for Efficient Photoelectrochemical Water Splitting. *Small* **2014**, *10* (18), 3692–3699. https://doi.org/10.1002/smll.201400276.
(S22) Amano, F.; Li, D.; Ohtani, B. Fabrication and Photoelectrochemical Property of Tungsten(vi) Oxide Films with a Flake-Wall Structure. *Chem. Commun.* **2010**, *46* (16), 2769–2771. https://doi.org/10.1039/b926931b.
(S23) Su, J.; Guo, L.; Bao, N.; Grimes, C. A. Nanostructured WO_3/$BiVO_4$ Heterojunction Films for Efficient Photoelectrochemical Water Splitting. *Nano Lett.* **2011**, *11* (5), 1928–1933. https://doi.org/10.1021/nl2000743.
(S24) Cristino, V.; Caramori, S.; Argazzi, R.; Meda, L.; Marra, G. L.; Bignozzi, C. A. Efficient Photoelectrochemical Water Splitting by Anodically Grown WO_3 Electrodes. *Langmuir* **2011**, *27* (11), 7276–7284. https://doi.org/10.1021/la200595x.
(S25) Santato, C.; Ulmann, M.; Àugustynski, J. Photoelectrochemical Properties of Nanostructured Tungsten Trioxide Films. *J. Phys. Chem. B* **2001**, *105* (5), 936–940. https://doi.org/10.1021/jp002232q.
(S26) Yang, B.; Zhang, Y.; Drabarek, E.; Barnes, P. R. F.; Luca, V. Enhanced Photoelectrochemical Activity of Sol-Gel Tungsten Trioxide Films through Textural Control. *Chem. Mater.* **2007**, *19* (23), 5664–5672. https://doi.org/10.1021/cm071603d.
(S27) Li, W.; Li, J.; Wang, X.; Luo, S.; Xiao, J.; Chen, Q. Visible Light Photoelectrochemical Responsiveness of Self-Organized Nanoporous WO_3 Films. *Electrochim. Acta* **2010**, *56* (1), 620–625. https://doi.org/10.1016/j.electacta.2010.06.025.
(S28) Chakrapani, V.; Thangala, J.; Sunkara, M. K. WO_3 and W_2N Nanowire Arrays for Photoelectrochemical Hydrogen Production. *Int. J. Hydrogen Energy* **2009**, *34* (22), 9050–9059. https://doi.org/10.1016/j.ijhydene.2009.09.031.

(S29) Qin, D. D.; Tao, C. L.; Friesen, S. A.; Wang, T. H.; Varghese, O. K.; Bao, N. Z.; Yang, Z. Y.; Mallouk, T. E.; Grimes, C. A. Dense Layers of Vertically Oriented WO_3 Crystals as Anodes for Photoelectrochemical Water Oxidation. *Chem. Commun.* **2012**, *48* (5), 729–731. https://doi.org/10.1039/c1cc15691h.

(S30) Hong, S. J.; Jun, H.; Borse, P. H.; Lee, J. S. Size Effects of WO_3 Nanocrystals for Photooxidation of Water in Particulate Suspension and Photoelectrochemical Film Systems. *Int. J. Hydrogen Energy* **2009**, *34* (8), 3234–3242. https://doi.org/10.1016/j.ijhydene.2009.02.006.

(S31) Meda, L.; Tozzola, G.; Tacca, A.; Marra, G.; Caramori, S.; Cristino, V.; Alberto, C. Solar Energy Materials & Solar Cells Photo-Electrochemical Properties of Nanostructured WO_3 Prepared with Different Organic Dispersing Agents. *Sol. Energy Mater. Sol. Cells* **2010**, *94* (5), 788–796. https://doi.org/10.1016/j.solmat.2009.12.025.

(S32) Gonçalves, R. H.; Leite, L. D. T.; Leite, E. R. Colloidal WO_3 Nanowires as a Versatile Route to Prepare a Photoanode for Solar Water Splitting. *ChemSusChem* **2012**, *5* (12), 2341–2347. https://doi.org/10.1002/cssc.201200484.

(S33) Kong, H.; Yang, H.; Park, J. S.; Chae, W. S.; Kim, H. Y.; Park, J.; Lee, J. H.; Choi, S. Y.; Park, M.; Kim, H.; Song, Y.; Park, H.; Yeo, J. Spatial Control of Oxygen Vacancy Concentration in Monoclinic WO_3 Photoanodes for Enhanced Solar Water Splitting. *Adv. Funct. Mater.* **2022**, *32* (36), 1–14. https://doi.org/10.1002/adfm.202204106.

(S34) Zhang, J.; Salles, I.; Pering, S.; Cameron, P. J.; Mattia, D.; Eslava, S. Nanostructured WO_3 Photoanodes for Efficient Water Splitting: Via Anodisation in Citric Acid. *RSC Adv.* **2017**, *7* (56), 35221–35227. https://doi.org/10.1039/c7ra05342h.

(S35) Jelinska, A.; Bienkowski, K.; Jadwiszczak, M.; Pisarek, M.; Strawski, M.; Kurzydlowski, D.; Solarska, R.; Augustynski, J. Enhanced Photocatalytic Water Splitting on Very Thin WO_3 Films Activated by High-Temperature Annealing. *ACS Catal.* **2018**, *8* (11), 10573–10580. https://doi.org/10.1021/acscatal.8b03497.

(S36) Shao, C.; Malik, A. S.; Han, J.; Li, D.; Dupuis, M.; Zong, X.; Li, C. Oxygen Vacancy Engineering with Flame Heating Approach towards Enhanced Photoelectrochemical Water Oxidation on WO_3 Photoanode. *Nano Energy* **2020**, *77* (May), 105190. https://doi.org/10.1016/j.nanoen.2020.105190.

(S37) Shin, S.; Han, H. S.; Kim, J. S.; Park, I. J.; Lee, M. H.; Hong, K. S.; Cho, I. S. A Tree-like Nanoporous WO_3 Photoanode with Enhanced Charge Transport Efficiency for Photoelectrochemical Water Oxidation. *J. Mater. Chem. A* **2015**, *3* (24), 12920–12926. https://doi.org/10.1039/c5ta00823a.

(S38) Wang, Y.; Zhang, F.; Zhao, G.; Zhao, Y.; Ren, Y.; Zhang, H.; Zhang, L.; Du, J.; Han, Y.; Kang, D. J. Porous WO_3 Monolith-Based Photoanodes for High-Efficient Photoelectrochemical Water Splitting. *Ceram. Int.* **2019**, *45* (6), 7302–7308. https://doi.org/10.1016/j.ceramint.2019.01.012.

(S39) Liu, Y.; Wygant, B. R.; Mabayoje, O.; Lin, J.; Kawashima, K.; Kim, J. H.; Li, W.; Li, J.; Buddie Mullins, C. Interface Engineering and Its Effect on WO_3-based Photoanode and Tandem Cell. *ACS Appl. Mater. Interfaces* **2018**, *10* (15), 12639–12650. https://doi.org/10.1021/acsami.8b00304.